

# THERMALLY INDUCED VIBRATION CONTROL OF COMPOSITE THIN-WALLED ROTATING BLADE

Sungsoo Na\*, Liviu Librescu\*\*, Hoedo Jung\*, Injoo Jeong\*  
 \*Korea University, \*\*VA Tech

**Keywords:** *thin-walled rotating beam, composite material, thermally induced vibration control*

## Abstract

*This paper deals with thermally induced dynamic response control analysis of a rotating composite blade, modeled as a tapered thin-walled beam induced by heat flux. The displayed results reveal that the thermal environment yields a detrimental repercussions upon their dynamic responses. The blade consists of host graphite epoxy laminate and spanwise distributed transversely isotropic (PZT-4) sensors and actuators. The controller is implemented via the combined negative displacement and velocity feedback control methodology, which prove to overcome the deleterious effect associated with the thermally induced dynamic response. The structure is modeled as a composite thin-walled beam incorporating a number of nonclassical features such as transverse shear, secondary warping, anisotropy of constituent materials, and rotary inertias.*

## 1 Introduction

The increasing use of fiber-reinforced, composite, thin-walled beam construction for rotor blades used in helicopter, tilt rotor aircraft, turbo engine, spacecraft boom and other applications, has generated a great deal of research activity aimed at enhancing their dynamic response performances. For reasons of efficiency involving gas dynamics and weight, they must be thin, yet to operate in severe thermal environments and at higher rotational speeds.

Boley[1] was the first to include inertia effects in calculating the thermal-structural

response of a beam subject to rapid heating and presented the governing equations for the problem of thermally induced vibrations. Seibert and Rice [2] investigated coupled thermoelastic effect for Euler-Bernoulli and Timoshenko beam model. Johnston and Thornton [3] analyzed the effects of thermally induced structural disturbances of an appendage on the dynamics of a simple spacecraft.

Thornton and Kim [4] developed an analytical approach to determine the thermal-structural response of a flexible rolled-up solar array due to a sudden increase in the external heating. The coupled thermal-structural responses were compared with the uncoupled analysis results. I. Yoon [5] investigated thermally induced vibration of composite thin-walled beam. The structure is modeled as a circular thin-walled beam of closed cross section and has constant cross area ratio.

Although of an evident importance, to the best of authors' knowledge, no such studies including thermally-induced dynamic response control of nonuniform composite thin-walled rotating blade, have been found. The rotating beam may be constitutes part of a rotating spacecraft boom.

Both the dynamic equations involving the temperature effects and the related boundary conditions are obtained via the application of Hamilton's variational principle. In its modeling the effects of anisotropy of constituent materials, transverse shear, warping, rotary inertia, etc are incorporated. In addition, in order to induce elastic couplings between flapwise bending and chordwise bending, a special ply-angle distribution achieved via the usual helically wounding fiber-reinforced technology is

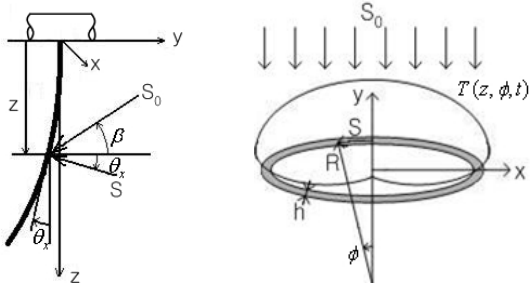
implemented. The numerical simulations display eigenfrequencies and deflection time-history as a function of the fiber orientation of the composite materials, rotating speed, taper ratio.

## 2 Thermal Analysis

### 2.1 Basic Assumptions

A thin-walled beam of radius  $R$  and wall thickness  $h$  is considered (Fig. 1). The blade is subjected to a known incident heat flux  $S$  applied at time  $t=0$ . The associated problem is to determine the transient temperature response of the tip of the blade. To this end, the following assumptions are adopted.

1. Heat is conducted only in the circumferential direction, implying that the heat conduction along the blade length is negligible,
2. Thermal energy losses at the cantilevered support at  $x=0$  are neglected, and thermal energy is emitted from external surface of the blade assuming diffuse radiation, but internal radiation within the blade is neglected,
3. The temperature field is assumed to be uniform across the beam thickness, implying that the temperature gradient across it is neglected,
4. Convection heat transfer inside and outside the beam is negligible,



(a) Heat Flux (b) Beam Cross Section

Fig.1 Heat flux for coupled thermal-structural analysis

### 2.2 Thermal Analysis

In such a context, the thermodynamic equation of heat conduction and radiation is

$$\frac{\partial T}{\partial t} - \frac{k}{\rho c R^2} \frac{\partial^2 T}{\partial \phi^2} + \frac{\sigma \varepsilon}{\rho c h} T^4 = \frac{\alpha S_0}{\rho c h} \delta \cos \phi \cos(\beta + \theta_x) \quad (1)$$

In Eq. (1),  $T \equiv (z, \phi, t)$  is the absolute temperature at an arbitrary point of beam,  $k$  is the thermal conductivity,  $\rho$  and  $c$  are the weight density and the specific heat of the material, respectively,  $t$  is time coordinate and  $\delta$  is unity for the values of circumferential coordinate  $\phi$  corresponding to the portion of beam surface exposed to radiation and zero otherwise. The heat flux intensity of radiation source at an angle  $\beta$  with respect to the direction normal to the undeflected beam axis,  $S_0$ , is related to the counterpart one at an arbitrary point of the deflected beam surface,  $S$ , by

$$S = S_0 \cos(\beta + \theta_x) \quad (2)$$

The thermodynamic equation of heat-conduction-radiation can be linearized. As a result, one can represent  $T$  as

$$T(z, \phi, t) = \bar{T} + T_1(z, \phi, t) \quad (3)$$

where  $T_1(z, \phi, t)$  is the disturbance temperature, and  $\bar{T}$  is the steady-state absolute temperature fulfilling the condition  $\bar{T} \square T_1(z, \phi, t)$ .

Further, we will consider

$$T_1(z, \phi, t) = \hat{T}(z, t) \cos \phi \quad (4)$$

where  $\hat{T}$  is the maximum disturbance temperature. As a result of Eq. (3),  $T^4(z, \phi, t)$  intervening in Eq. (1) is expressed as a truncated binomial series expansion about  $\bar{T}$  in the form

$$T^4(z, \phi, t) \approx \bar{T}^4 + 4\bar{T}^3 \hat{T}(z, t) \cos \phi \quad (5)$$

Moreover, the heat flux distribution on the right of Eq. (1) is represented as:

$$\delta \cos \phi = \frac{3}{2\pi} + \left( \frac{1}{2} + \frac{3\sqrt{3}}{4\pi} \right) \cos \phi \quad (6)$$

By virtue of Eqs. (5) and (6), from Eq. (1) one obtains

$$\bar{T}_{ss} = \left( \frac{3}{2\pi} \frac{\alpha S_0 \cos \beta}{\sigma \varepsilon} \right)^{1/4} \quad (7)$$

and

$$\frac{\partial \hat{T}}{\partial t} + \frac{1}{\tau} \hat{T} = \frac{T^*}{\tau} \cos(\beta + \theta_x) \quad (8)$$

where

$$\frac{1}{\tau} = \frac{k}{\rho c R^2} + \frac{4\sigma \varepsilon \bar{T}^3}{\rho c h}, T^* = \left( \frac{1}{2} + \frac{3\sqrt{3}}{4\pi} \right) \frac{\sigma S_0}{\rho c h} \tau \quad (9)$$

denote a characteristic time and the time-independent maximum disturbance temperature, respectively, when the blade is deflected statically. Assuming zero initial conditions, from Eq. (8) one obtains

$$\hat{T}(z, t) = \frac{e^{-t/\tau} T^*}{\tau} \int_0^t e^{p/t} \cos(\beta + \theta_x) dp \quad (10)$$

where  $p$  is a dummy time variable. It is readily seen that the disturbance temperature as expressed by Eq. (10) depends nonlinearly on  $\theta_x$ . Assuming  $\theta_x$  to be small, one can linearize  $\hat{T}(z, t)$  as to become

$$\hat{T}(z, t) = \frac{e^{-t/\tau} T^*}{\tau} \int_0^t e^{p/t} (\cos \beta - \sin \theta_x) dp \quad (11)$$

### 3 Formulation of The Composite Thin-Walled Beam Model

#### 3.1 Basic Assumptions and Kinematics of the Modeling Formulation

The tapered composite blade consisting of a single cell thin-walled beam is mounted on a rigid hub (radius  $R_0$ ) that rotates with constant angular velocity  $\Omega$  about origin  $O$  (Fig. 2).

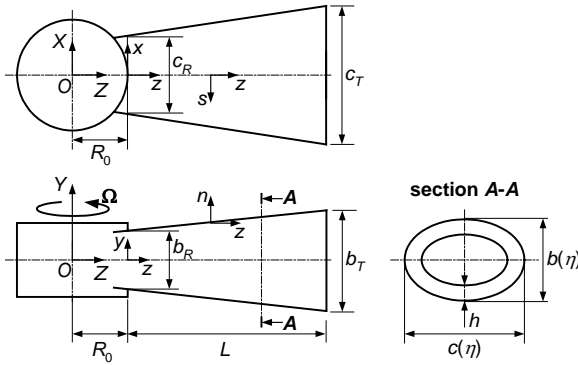


Fig.2 Geometric Configuration of the Rotating Blade

The inertial reference system  $(X, Y, Z)$  is attached to the center of the hub  $O$ . By  $(\mathbf{i}, \mathbf{j}, \mathbf{k})$  and  $(\mathbf{I}, \mathbf{J}, \mathbf{K})$ , we define the unit vectors associated with the coordinate systems  $(x, y, z)$  and  $(X, Y, Z)$ , respectively. The equations of rotating thin-walled beam are based on the following statements [6, 7, 8]:

(i) the original cross-section of the beam is preserved; (ii) the secondary warping effects are included; (iii) transverse shear, Coriolis effect, and centrifugal acceleration are incorporated; and finally, (iv) the constituent material of the structure features thermomechanical anisotropic properties.

The linear distribution of the chord  $c(\eta)$  and height  $b(\eta)$  of the mid-line cross-section profiles along the beam span is considered as

$$\begin{Bmatrix} c(\eta) \\ b(\eta) \end{Bmatrix} = [1 - \eta(1 - \sigma)] \begin{Bmatrix} c_R \\ b_R \end{Bmatrix} \quad (12)$$

Herein  $\sigma \equiv c_T / c_R$  denotes the taper ratio,  $\eta \equiv z / L$  is the dimensionless spanwise coordinate, where  $L$  denotes the beam semi-span, and subscripts  $R$  and  $T$  identify its characteristics at the root and tip cross-sections, respectively. In the same context, the radius of curvature of the circular arc associated with the midline contour at section  $\eta$  along the beam span varies according to the relationship:

$$R(\eta) = [1 - \eta(1 - \sigma)] R_R \quad (13)$$

The points of the beam cross-sections are identified by the global coordinates  $x, y$  and  $z$ , where  $z$  is the spanwise coordinate and by a local one,  $n, s$ , and  $z$ , where  $n$  and  $s$  denote the thicknesswise coordinate normal to the beam mid-surface and the tangential one along the contour line of the beam cross-section, respectively. (see Fig. 2)

In accordance with the above assumptions and in order to reduce the 3-D problem to an equivalent 1-D, the components of the displacement vector are expressed as [6]

$$\begin{aligned} u(x, y, z, t) &= u_0 - y\phi(z, t) \\ v(x, y, z, t) &= v_0 + x\phi(z, t) \\ w(x, y, z, t) &= w_0(z, t) + \theta_x(z, t)[y(s) - n \frac{dx}{ds}] + \end{aligned} \quad (14)$$

$$\theta_y(z, t)[x(s) + n \frac{dy}{ds}] - \phi'(z, t)[F_w(s) + na(s)]$$

$$\theta_x(z, t) = \gamma_{yz}(z, t) - v_0'(z, t) \quad (15)$$

$$\theta_y(z, t) = \gamma_{xz}(z, t) - u_0'(z, t)$$

Eqs. (14) and (15) reveal that the kinematic variables,  $u_0(z,t)$ ,  $v_0(z,t)$ ,  $w_0(z,t)$ ,  $\theta_x(z,t)$ ,  $\theta_y(z,t)$  and  $\phi(z,t)$  representing three translations in the  $x$ ,  $y$ ,  $z$  directions and three rotations about the  $x$ ,  $y$ ,  $z$  directions, respectively are used to define the displacement components,  $u$ ,  $v$  and  $w$ , while following coordinates description,  $\theta_x(z,t)$  and  $\theta_y(z,t)$  denote the rotations about axes  $x$  and  $y$  respectively, while  $\gamma_{yz}$  and  $\gamma_{xz}$  denote the transverse shear in the planes  $yz$  and  $xz$  respectively and the primes denote derivatives with respect to the  $z$ -coordinate, respectively.

Notice that the  $z$  - axis is located as to coincide with the locus of symmetrical points of the cross-section along the wing span.

The kinetic energy  $K$ , and potential energy  $V$ , expressions for a beam are

$$K = \frac{1}{2} \int_{\tau} \rho (\dot{\mathbf{R}}_i \cdot \dot{\mathbf{R}}_i) d\tau \quad (16)$$

$$V = \frac{1}{2} \int_{\tau} \sigma_{bij} \varepsilon_{bij} d\tau \\ = \frac{1}{2} \int_0^L \oint_C \sum_{k=1}^N \int_{h(k)} [\sigma_{bzz} \varepsilon_{bzz} + \sigma_{bsz} \gamma_{bsz} + \sigma_{bnz} \gamma_{bnz}]_{(k)} dnds dz$$

The expressions for the virtual work done by externally applied forces are

$$\delta W_f = \int_0^L f(z,t) \delta v(z,t) dz \quad (17)$$

In these equations  $d\tau (\equiv dnds dz)$  denotes the differential volume element and the position vector  $\mathbf{R} \equiv \mathbf{R}(x,y,z,t)$  relative to a fixed origin is defined as:

$$\mathbf{R} = \mathbf{R}_0 + \mathbf{r} + \Delta \quad (18)$$

In Eq. (18),  $\mathbf{r} (\equiv xi+yj+zk)$  defines the undeformed position of a point measured in the beam coordinate system and  $\Delta (\equiv ui+vj+wk)$  denotes the displacement vectors of the points of the blades, while  $\mathbf{R}_0 = R_0 \mathbf{k}$ .

### 3.2 The Equations of Motion and Boundary conditions

Employment of constitutive equations and strain-displacement relationships in the Eq. (16), and carrying out the indicated integrations with respect to  $n$  and  $s$ , one can obtain simplified kinetic and potential energy, which is applied to the extended Hamilton's principle in order to obtain the coupled bending equations of

adaptive rotating beams and the associated boundary conditions.

$$\int_{t_0}^{t_1} (\delta K - \delta V + \delta W) dt = 0 \quad (19) \\ \delta u_0 = \delta v_0 = \delta \theta_x = \delta \theta_y = 0 \quad \text{at } t = t_1, t_2$$

Herein  $K$  and  $V$  denote the kinetic and strain energy, respectively,  $\delta W$  is the virtual work of external forces,  $t_1$  and  $t_2$  are two arbitrary instants of time, while  $\delta$  is the variational operator.

The Equations governing the (flap-lag) Bending-Transverse Shear Motion:

$$[a_{43} \theta'_x + a_{44} (u'_0 + \theta_y)]' + \Omega^2 \{P(z) u'_0\}' - b_1 \Omega^2 u_0 - b_1 \ddot{u}_0 - h_4^{T'} = 0, \\ [a_{52} \theta'_y + a_{55} (v'_0 + \theta_x)]' + \Omega^2 \{P(z) v'_0\}' - b_1 \ddot{v}_0 - h_5^{T'} = 0, \\ [a_{22} \theta'_y + a_{25} (v'_0 + \theta_x)]' - a_{44} (u'_0 + \theta_y) - a_{43} \theta'_x \\ - (b_5 + b_{15}) (\ddot{\theta}_y - \Omega^2 \theta_y) - h_2^{T'} + h_4^T = 0, \\ [a_{33} \theta'_x + a_{34} (u'_0 + \theta_y)]' - a_{55} (v'_0 + \theta_x) - a_{52} \theta'_y \\ - (b_4 + b_{14}) (\ddot{\theta}_x - \Omega^2 \theta_x) - h_3^{T'} + h_5^T = 0 \quad (20a-d)$$

The associated BCs for the rotating beams clamped at  $z=0$  and free at  $z=L$  are:

$$\text{At } z=0, \quad u_0 = v_0 = \theta_y = \theta_x = 0 \quad (21a-d)$$

At  $z=L$ ,

$$a_{43} \theta'_x + a_{44} (u'_0 + \theta_y) = h_4^T, \\ a_{52} \theta'_y + a_{55} (v'_0 + \theta_x) = h_5^T, \quad (22 a-d) \\ a_{22} \theta'_y + a_{25} (v'_0 + \theta_x) = h_2^T - M_y^{a'}, \\ a_{33} \theta'_x + a_{34} (u'_0 + \theta_y) = h_3^T - M_x^{a'}$$

In Eqs. (20) through (22),  $a_{ij}$ ,  $b_i$  denote global stiffness and mass quantities, respectively.  $P(z)$  is obtained as

$$P(z) = \int_z^L b_1(z) (R_0 + z) dz \quad (23)$$

and  $h_i^T (\equiv h_i^T(z,t))$  denote the thermal stress-resultants and thermal stress-couples defined as:

$$h_2^T = \oint_C (x N_1^T + \frac{dy}{ds} N_4^T) ds, \quad h_4^T = \oint_C N_2^T \frac{dx}{ds} ds \\ h_3^T = \oint_C (y N_1^T - \frac{dx}{ds} N_4^T) ds, \quad h_5^T = \oint_C N_2^T \frac{dy}{ds} ds \quad (24a-d)$$

### 3.3 Piezoelectric Distribution and the Control Law

For the general case, the expression of the piezoelectrically induced flap and lag bending moment is given by, respectively

$$\begin{aligned} M_x^{a'}(z,t) &= C_x V(t) [H(z-z_1) - H(z-z_2)] \\ M_y^{a'}(z,t) &= C_y V(t) [H(z-z_1) - H(z-z_2)] \end{aligned} \quad (25a,b)$$

where  $C_x, C_y$  are constants dependent on the mechanical and geometrical properties of the piezoactuator and host structure and  $V(t)$  is the applied input voltage that is equal and opposite in sign in the upper and lower piezoactuators (out-of-phase actuation).  $H(\cdot)$  denotes the Heaviside function representing the actuator distribution. (Fig. 3)

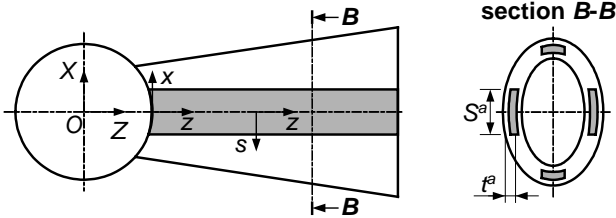


Fig. 3 Distribution of Piezoactuators

In the previously displayed equations, due to the special distribution of piezoactuators, it was shown that the piezoelectrically induced moment intervenes solely in the boundary conditions associated with the bending motion, prescribed at the beam tip, and hence it plays the role of the boundary moment control. Within the adopted feedback control law the piezoelectrically induced bending moment at the blade tip is expressed as

$$\begin{aligned} M_x^{a'}(L) &= k_{vx} \dot{\theta}_x(L) + k_{px} \theta_x(L) \\ M_y^{a'}(L) &= k_{vy} \dot{\theta}_y(L) + k_{py} \theta_y(L) \end{aligned} \quad (26a,b)$$

Herein  $k_x, k_y$  denote the feedback gains, and in the numerical simulations nondimensional counterpart of  $k_x, k_y$  is  $K_x, K_y$  defined by

$$\begin{aligned} K_{vx} &= k_{vx} L^2 / a_{33}^0, & K_{px} &= k_{px} L^2 / a_{33}^0 \\ K_{vy} &= k_{vy} L^2 / a_{22}^0, & K_{py} &= k_{py} L^2 / a_{22}^0 \end{aligned} \quad (27a,b)$$

#### 4. Results and Discussions

A numerical study was performed to investigate the quasi-static and the dynamic response of the system consisting of a rotating

composite thin-walled blade exposed to an incident heat flux applied instantaneously at  $t=0$ . The data on which basis the numerical simulations have been generated are supplied in Table 1.

Figs. 4 and 5 show the average, perturbation temperature response of the composite blade, while Fig. 6 displays temperature distribution along the blade cross-section from the uncoupled analysis. Fig. 4 shows average temperature  $\bar{T}$  is approximately 330.8K, when  $T_0$  is 290K. Temperature profiles for the upper one-half of the blade cross-section at various times are shown in Fig. 6, which proves the development of the blade thermal gradients.

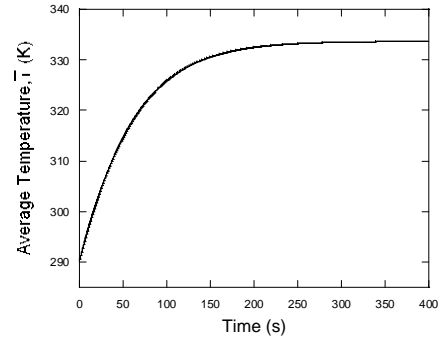


Fig.4 Average temperature response of a composite blade

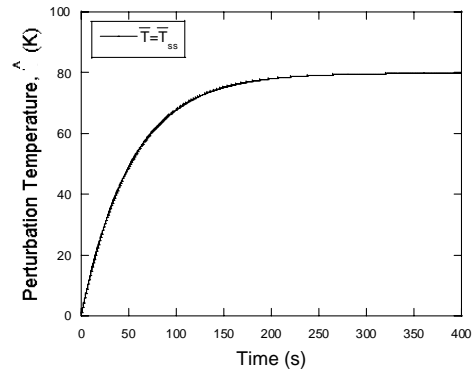


Fig. 5 Perturbation temperature response of a composite blade

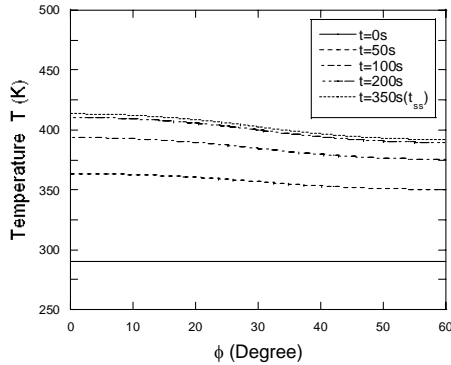


Fig.6 Temperature distribution for a composite blade

From Figs. 7 to 9 the plots highlight the effects of angular velocity, taper ratio and ply angle orientation on the natural frequencies of the coupled flap-lag bending motion. From the results it becomes evident that as the beam taper increases (i.e. when  $\sigma$  goes above 1.0) the first and second coupled natural frequencies decrease whereas the third one increases. The plots also display the sensitivity of natural frequencies to ply angle orientation. A general remark emerging from Figs. 7 to 9 is that the stiffening effect due to beam rotation contributes to the increase of natural frequencies for all taper ratios.

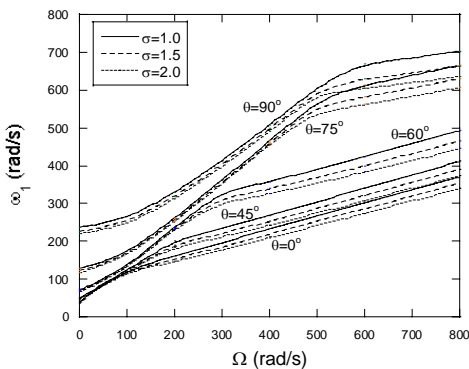


Fig. 7 First coupled flap-lag bending frequency vs.  $\Omega$  for different ply angles

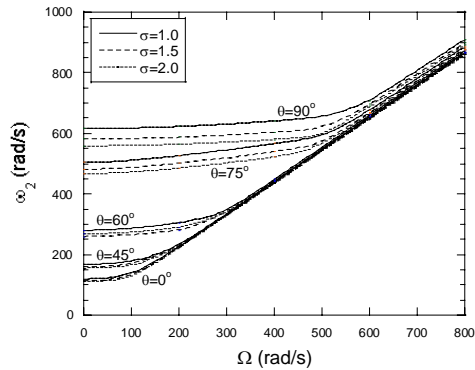


Fig. 8 Second coupled flap-lag bending frequency vs.  $\Omega$  for different ply angles

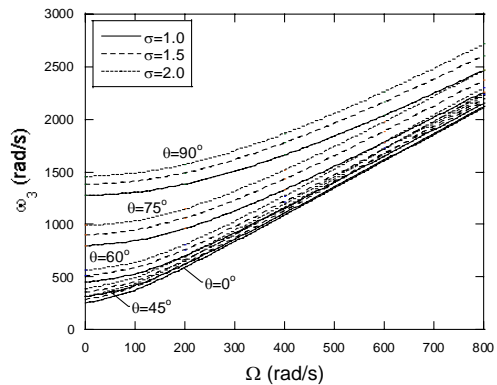


Fig. 9 Third coupled flap-lag bending frequency vs.  $\Omega$  for different ply angles

Figs. 10 and 11 highlight the effect of the incident angle of heat flux and of taper ratio on the dynamic response behavior. The results reveal that taper ratio plays a significant role in confining the deflection response and the increase of incidence angle can decrease both the flapwise and chordwise response.

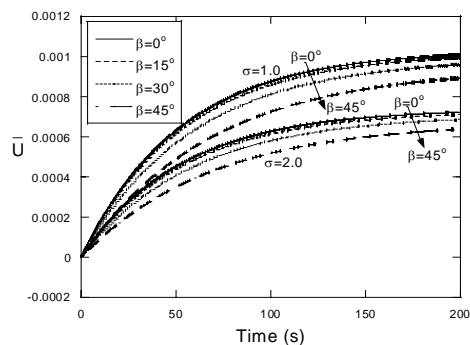


Fig. 10 Nondimensional flapping response for various heat incident angle,  $\theta=30^\circ$ ,  $\Omega=200$  rad/s

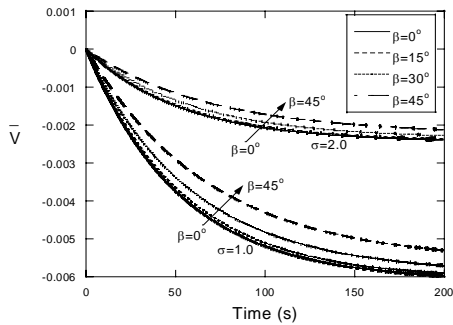


Fig. 11 Nondimensional flapping response for various heat incident angle,  $\theta=30^\circ$   $\Omega=200$  rad/s

Fig. 12 displays the time-history of transversal deflection response. This graph highlights the strong effect played by the angular velocity to flapping dynamic response.

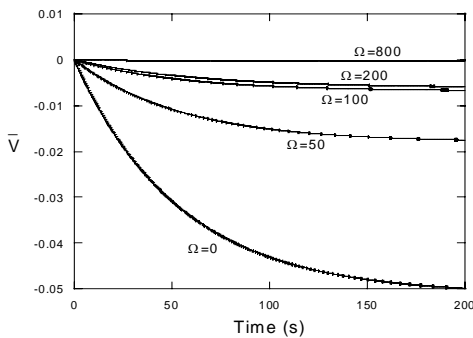


Fig. 12 Nondimensional flapping response for various angular velocity,  $\sigma=2$ ,  $\theta=30^\circ$   $\beta=15^\circ$

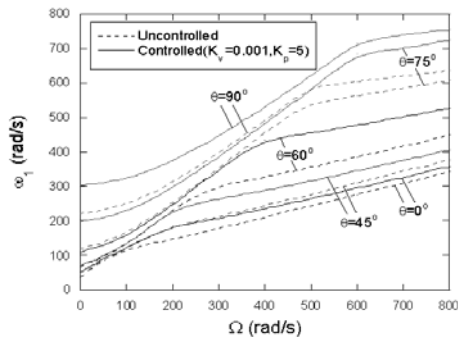


Fig. 13 Uncontrolled and controlled first coupled flap-lag bending frequency vs.  $\Omega$  for different ply angles,  $\sigma=2$

In Figs. 13 through 15 there are depictions of the effects of angular velocity and ply angle orientation on the uncontrolled and controlled natural frequencies of the coupled flap-lag bending motions. The results reveal the potential role played by the piezoelectric actuation upon the enhancement of eigenfrequencies. Figs 16 and 17 displayed uncontrolled and controlled time history of lagging and flapping response of a blade subjected to heat flux, respectively. The results reveal negative displacement feedback control provides a powerful tool for improved structural responses, relatively, in low range of angular velocity

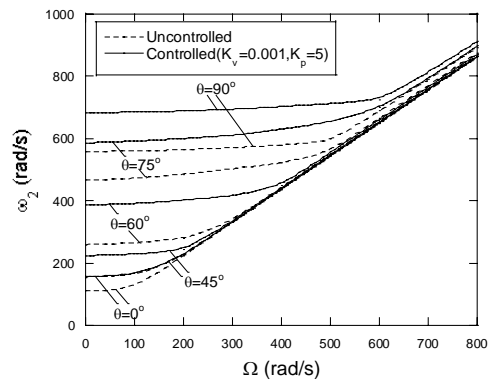


Fig. 14 Uncontrolled and controlled second coupled flap-lag bending frequency vs.  $\Omega$  for different ply angles,  $\sigma=2$

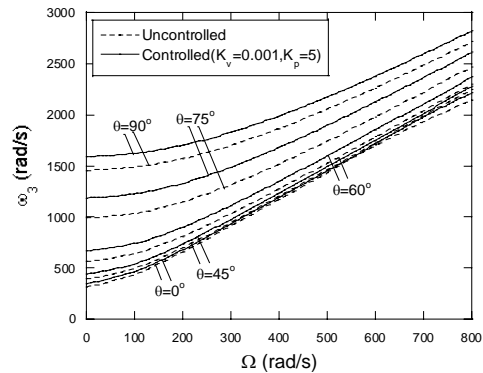


Fig. 15 Uncontrolled and controlled third coupled flap-lag bending frequency vs.  $\Omega$  for different ply angles,  $\sigma=2$

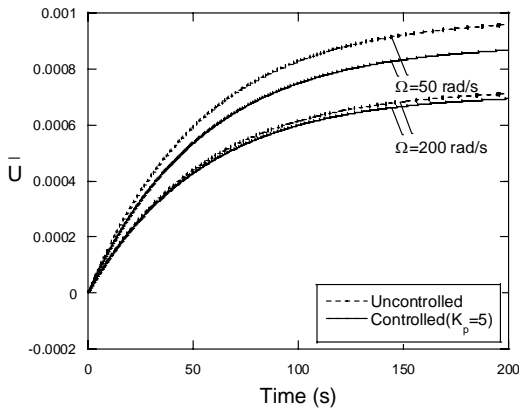


Fig. 16 Uncontrolled and controlled lagging response for various angular velocity,  $\sigma=2$ ,  $\theta=30^\circ$ ,  $\beta=15^\circ$

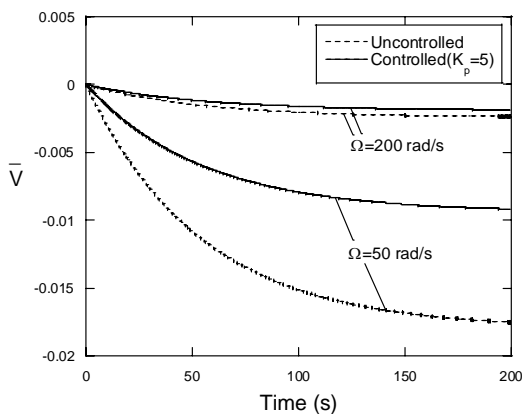


Fig. 17 Uncontrolled and controlled flapping response for various angular velocity,  $\sigma=2$ ,  $\theta=30^\circ$ ,  $\beta=15^\circ$

## 5. Conclusions

A comprehensive structural model of composite thin-walled rotating blade was developed and the problem of the thermally induced vibration was addressed.

The effects of the heat incident angle, rotating speed, blade taper ratios and ply angles of composite materials to the dynamic response of the blade structure are studied by using the coupled thermal-structural analysis. The implications of a number of factors such as

blade taper ratios, ply angles of composite materials, rotational speed, heat incident angle and piezoelectric actuation may improve the quasi-static and dynamic deflection of the blade.

## Acknowledgment

Sungsoo Na would like to acknowledge the financial support by the Basic Research Program of the Korea Science & Engineering Foundation, Grant No. R01-2002-000-00129-0.

## References

- [1] B. A. Boley, J. H. Weiner, "Theory of Thermal Stress," *John Wiley & Sons, Inc.*, pp 3-355, 1960.
- [2] A. G. Seibert, J. S. Rice, "Coupled Thermally Induced Vibrations and Beams," *AIAA Journal*, Vol. 7, No. 7, pp.1033-1035, 1973.
- [3] J. D. Johnson, E. A. Thornton, "Thermally Induced Attitude Dynamics of a Spacecraft with Flexible Appendage," *Journal of Guidance, Control and Dynamics*, Vol. 21, No. 4, pp 581-587, 1998.
- [4] E. A. Thornton, Y. A. Kim, "Thermally Induced Bending Vibration of a Flexible Rolled-Up Solar Array," *Journal of Spacecraft and Rockets*, Vol. 30, No. 4, pp 438-448, 1993.
- [5] I. Yoon, "Thermally Induced Bending Vibration of Composite Spacecraft Booms Subjected to Solar Heating," Ph. D Thesis, Chung-Nam National University, Korea.
- [6] Song, O. and Librescu, L., "Structural Modeling and Free Vibration Analysis of Rotating Composite Thin-Walled Beams," *J. of the American Helicopter Society*, Vol. 42, No. 4, pp 358-369, 1997.
- [7] Song, O., Librescu, L. Oh, S.Y., "Dynamics of Pretwisted Rotating Thin-Walled Beams Operating in a Temperature Environment," *Journal of Thermal Stresses*, Vol. 24, pp 255-279, 2001.
- [8] Na, S., and Librescu, L., "Modeling and Vibration Feedback Control of Rotating Tapered Beams Incorporating Adaptive Capabilities," *ASME 2000, PVP-Vol. 415, Recent Advances in Solids and Structures*, pp 35-53, 2000.
- [9] O. Song, "Modeling and Response Analysis of Thin-Walled Beam Structures Constructed of Advanced Composite Materials," Ph. D Thesis, VPI&SU, USA.
- [10] M. Murozono, S. Sumi, "Thermally-Induced Bending Vibration of Thin-Walled Beam with Closed Section Caused by Radiant Heating," *Memoirs of the faculty of Engineering, Kyushu University*, Vol. 49, No. 4, pp 273-290, 1989.
- [11] S. S. Na, "Control of Dynamic Response of Thin-Walled Composite Beams Using Structural Tailing and Piezoelectric Actuation," Ph. D Thesis, VPI&SU, USA, 1997.

Appendix

Table. 1 Material and geometric properties of composite material (Graphite/Epoxy)

Parameter	Value
$L$	2.032 m
$h$	2.35E-4 m
$R$	0.254 m
$E_1$	2.068E11 N/m <sup>2</sup>
$E_2=E_3$	5.171E9 N/m <sup>2</sup>
$G_{12}$	3.103E9 N/m <sup>2</sup>
$G_{23}=G_{31}$	2.551E9 N/m <sup>2</sup>
$\mu_{12}=\mu_{23}=\mu_{13}$	0.25
$\rho$	1528.227 kg/m <sup>3</sup>
$\alpha$	0.92
$\alpha_1$	1.1E-6 K <sup>-1</sup>
$\alpha_2$	25.2E-6 K <sup>-1</sup>
$\varepsilon$	0.84
$\sigma$	5.67E-8 W/m <sup>2</sup> K <sup>4</sup>
$k$	1.731 W/mK
$c$	1044 J/kgK
$S_0$	1.35E3 W/m <sup>2</sup>